Rigorously solvable model for the electrical conductivity of dispersions of hard-core–penetrable-shell particles and its applications

M. Ya. Sushko ◉[*] and A. K. Semenov

Department of Theoretical Physics and Astronomy, Mechnikov National University, 2 Dvoryanska Street, Odesa 65026, Ukraine

We generalize the compact group approach to conducting systems to give a self-consistent analytical solution to the problem of the effective quasistatic electrical conductivity of macroscopically homogeneous and isotropic dispersions of hard-core–penetrable-shell particles. The shells are in general inhomogeneous and characterized by a radially symmetrical, piecewise-continuous conductivity profile. The local value of the conductivity is determined by the shortest distance from the point of interest to the nearest particle. The effective conductivity is expressed in terms of the constituents' conductivities and volume concentrations; the latter account for the statistical microstructure of the system. The theory effectively incorporates many-particle effects and is expected to be rigorous in the static limit. Using the well-tested statistical physics results for the shell volume concentration, this conclusion is backed up by mapping the theory on available 3D random resistor network simulations for hard spheres coated with fully penetrable concentric shells. Finally, the theory is shown to fit experimental data for real composite solid electrolytes. The fitting results indicate that the effect of enhanced electrical conduction is generally contributed to by several mechanisms. These are effectively taken into account through the shell conductivity profile.

I. INTRODUCTION

The objectives of this paper are threefold: (1) to develop a homogenization theory for the effective quasistatic electrical conductivity σ_{eff} of macroscopically homogeneous and isotropic particulate substances and dispersions of particles with the core-shell morphology; (2) to test the theory by comparing its predictions with available results of random resistor network (RRN) simulations; and (3) to exemplify the applicability of the theory to real systems by processing experimental data for composite solid electrolytes (CSEs) prepared by dispersing fine insulating particles into matrix ionic conductors.

The indicated class of composites attracts a special attention due to nontrivial behavior of their σ_{eff}. Through the addition of filler particles (for instance, alumina particles, with electrical conductivity $\sigma_1 \sim 10^{-14}$ S/cm) to matrix ionic conductors (such as polycrystalline metal halides, whose typical electrical conductivities $\sigma_0 \sim 10^{-10} \div 10^{-5}$ S/cm), σ_{eff} of the resulting CSEs can be increased dramatically, by one to three orders of magnitude as compared to σ_0. This effect is called enhanced ionic conduction. Since its discovery by Liang [1] in polycrystalline lithium iodide containing alumina particles, it has been observed in dozens of CSEs (for a detailed bibliography, see reviews [2–9]) and composite polymer-based electrolytes [10,11] to make those promising materials for electrolytic applications.

Experiment also reveals that the maximum conduction enhancement usually occurs as the filler volume concentration

c reaches values in between 0.1 and 0.4. It is followed by a decrease in σ_{eff} as c is further increased. Such a nonmonotonic dependence of σ_{eff} upon c is a challenging problem for homogenization theory, since the existing approaches to two-phase systems, such as the classical Maxwell-Garnett [12,13] and Bruggeman [14,15] mixing rules, their numerous modifications (see Refs. [16–21]), cluster expansions [22,23] for dispersions of spheres with arbitrary degree of impenetrability, their extensions [24] with the Padé approximant technique, and systematic simulations [25–28] of random 2D systems of hard-core–penetrable-shell discs by combining Monte Carlo algorithms and finite element calculations do not exhibit it. The reason is that two-phase models oversimplify the actual microstructure of CSEs and disregard the processes involved.

A typical way out is to model a CSE as a three-phase system and determine σ_{eff} by solving a pertinent homogenization problem. The solution is expressed in terms of the geometric and electric parameters of the phases. These parameters are estimated so as to incorporate the relevant physical effects and account for the observed behavior of σ_{eff}. Several classes of such models have been proposed.

(i) Cubic lattices of cubic insulators surrounded by highly conductive layers and embedded in a conductive material [29–31]. The arrangement of particles on a simple cubic lattice makes it possible to represent the system with a resistor network and to calculate σ_{eff} for the entire range of c. The results suggest that the conductivity in the layer outside each particle may have a maximum at certain distance away from the surface.

(ii) Three-component resistor models with a matrix represented by normally conducting bonds, the inert randomly
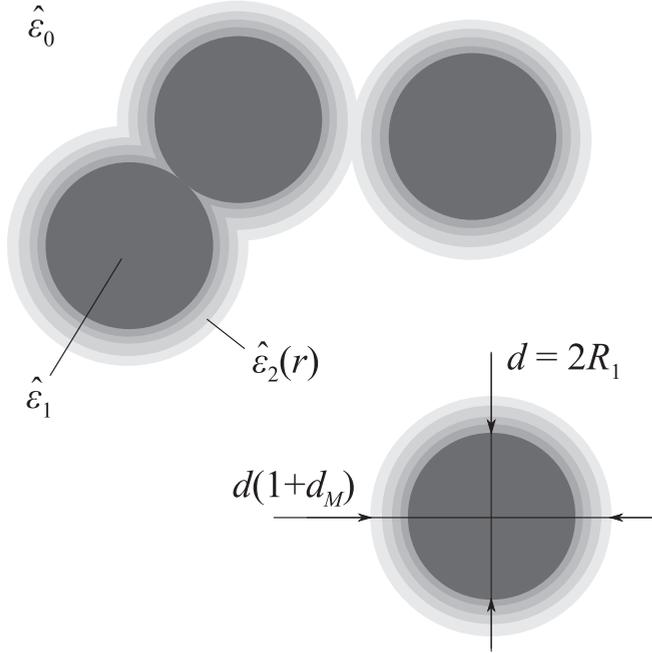
---
[*]mrs@onu.edu.ua

FIG. 1. The model under consideration. Each dispersed particle consists of a spherical hard core (shown black) with diameter $d = 2R_1$ and complex permittivity $\hat{\varepsilon}_1$. The core is coated with an isotropic (generally inhomogeneous) penetrable concentric shell (graded gray) with outer diameter $D = d(1 + \delta_M)$, relative thickness $\delta_M = (D - d)/d$, and complex permittivity profile $\hat{\varepsilon}_2 = \hat{\varepsilon}_2(r)$. The particles are embedded in a uniform matrix (white) with complex permittivity $\hat{\varepsilon}_0$. All the permittivities have form (5). The local value of the permittivity is determined by the shortest distance from the point of interest to the nearest particle.

distributed (quadratic or cubic) particles by insulating bonds, and the interface region by highly conducting bonds [32–34]. The models are solved by Monte Carlo simulations or a position-space renormalization technique and exhibit two threshold concentrations of the insulating material. One corresponds to the onset of interface percolation and the second one to a conductor-insulator transition. The effective medium and continuum percolation approaches to these models are discussed in Refs. [35] and [36,37], respectively.

(iii) Random three-phase dispersions of spherical particles comprising hard cores coated with concentric shells, either hard or penetrable (see Fig. 1), of potentially higher conductivity. Such core-shell models better suit the physical conditions in CSEs, but are harder to analyze. Analytical studies, such as [38–43], of them are usually limited to the case of hard shells, involve a sequence of one-particle approximations, and repeatedly use the Maxwell-Garnett [12,13] and/or Brugge-man [14,15] mixing rules. The case of penetrable shells has been attacked through RRN simulations, such as [44–46] for mono- and [47] for polysized particles. The essential details of these core-shell model results are scrutinized in Sec. VIII.

In what follows, we derive a self-consistent analytic many-particle solution for σ_{eff} of macroscopically homogeneous and isotropic 3D model dispersions of hard-core–penetrable-shell spheres, the shells being, in the general case, electrically inhomogeneous and characterized by radially-symmetrical,

piecewise-continuous conductivity profiles (see Fig. 1 for the details of the model). The desired σ_{eff} is a functional of the constituents' conductivities and volume concentrations that satisfies a certain integral relation, rigorous in the static limit. The volume concentrations account for the statistical microstructure of the system.

The derivation is carried out using the compact groups approach (CGA) [48–51]. It was originally designed to efficiently take into account many-particle polarization and correlation effects, without an in-depth modeling of those, in concentrated dielectric dispersions. In this paper, elaborating its statistical-averaging version, we (1) generalize the CGA to conducting systems whose constituents have complex permittivities with first-order poles at frequency $\omega = 0$; (2) scrutinize, for such systems, the passage to the (quasi)static limit $\omega \rightarrow 0$ in all terms of the iterative series for the averaged electric field and current; (3) bring new arguments, not restricted to dielectric systems, for the internally-consistent closure of the homogenization procedure and determination of the complex permittivity of the auxiliary host matrix; and (4) propose a technique for dealing with inhomogeneous overlapping regions.

Using the well-tested statistical physics results [52–54] for the shell volume concentration, we then validate the solution obtained by mapping it onto the entire set of available 3D random resistor network simulation data [44–46] for dispersions of hard spheres coated with fully penetrable (electrically uniform or inhomogeneous) concentric shells. The solution is capable of recovering all of these data in the entire ranges of c simulated. To our best knowledge, no such an analytic solution has been offered so far even for the simplest case of uniform shells with their conductivity being equal to that of the cores.

Finally, we apply the model to real CSEs. The results of processing experimental data [1] clearly indicate that the concept of inhomogeneous penetrable shells provides an efficient way for describing the net effect on σ_{eff} by different mechanisms. The latter may contribute most significantly in different ranges of c. If so, then they are accounted for by different parts in the model shell conductivity profile. This fact opens new opportunities for scrutinizing the physics of processes in real composites, which is of crucial importance in the situation where the consensus of opinions regarding the nature of ionic conduction enhancement in various composites has not been reached as yet [6–9].

The paper is arranged as follows. Some basic equations and definitions of macroscopic electrodynamics for media with complex permittivities of the constituents are recalled in Sec. II. With those in mind, the CGA is generalized in Sec. III to the problem of the effective quasistatic complex permittivity $\hat{\varepsilon}_{\text{eff}}$ of macroscopically homogeneous and isotropic dispersions. The governing equation for $\hat{\varepsilon}_{\text{eff}}$ is expressed in terms of the statistical moments $\langle [\delta \hat{\varepsilon}(\mathbf{r})]^s \rangle$ for the local deviations of the permittivity distribution in the dispersion from the complex permittivity $\hat{\varepsilon}_{\text{f}}$ of the host in the auxiliary system. By requiring that the CGA and boundary conditions [55] for complex electric fields be compatible, $\hat{\varepsilon}_{\text{f}}$ is determined in Sec. IV. The calculations of $\langle [\delta \hat{\varepsilon}(\mathbf{r})]^s \rangle$ for dispersions of isotropic core-shell particles with electrically homogeneous and inhomogeneous shells are performed in Secs. V and VI,

respectively. The resultant equations for σ_{eff} are presented in Sec. VII. Their validity is shown in Sec. VIII by mapping their solutions onto extensive RRN simulation data [44–46]. The applicability of the theory to real LiI/Al$_2$O$_3$ CSEs [1] is discussed in Sec. IX. The main results of the paper are summarized in Sec. X.

II. BASIC EQUATIONS AND DEFINITIONS

Consider the electromagnetic field caused in a nonmagnetic heterogeneous medium by time-harmonic ($\sim e^{-i\omega t}$, i being the imaginary unit) probing radiation whose working frequencies ω are sufficiently small to neglect any dielectric relaxation phenomena. The relevant frequency-domain Maxwell's macroscopic equations, written in the Gaussian units, have the form

$$\text{div}\,\mathbf{D} = 4\pi\rho, \quad \text{div}\,\mathbf{H} = 0, \tag{1}$$

$$\text{curl}\,\mathbf{E} = i\frac{\omega}{c}\mathbf{H}, \quad \text{curl}\,\mathbf{H} = \frac{4\pi}{c}\mathbf{j} - i\frac{\omega}{c}\mathbf{D}, \tag{2}$$

where $\mathbf{E}$, $\mathbf{D}$, $\mathbf{H}$, ρ, and $\mathbf{j}$ are the amplitude distributions of the electric field, electric displacement, magnetic field, free charge density, and free current density, respectively, and c is the speed of light in vacuum. The densities ρ and $\mathbf{j}$ are related by the continuity equation

$$-i\omega\rho + \text{div}\,\mathbf{j} = 0. \tag{3}$$

Assuming the standard linear constitutive equations

$$\mathbf{D} = \varepsilon\mathbf{E}, \quad \mathbf{j} = \sigma\mathbf{E}, \tag{4}$$

where $\varepsilon = \varepsilon(\mathbf{r})$ and $\sigma = \sigma(\mathbf{r})$ are the local (real) dielectric constant and electrical conductivity in the medium, one can introduce the quasistatic complex permittivity

$$\hat{\varepsilon} = \varepsilon + i\frac{4\pi\sigma}{\omega} \tag{5}$$

of the medium to obtain from Eqs. (1)–(4) the equation for the quasistatic electric field distribution

$$\Delta\mathbf{E} + k_0^2\hat{\varepsilon}\,\mathbf{E} - \text{grad}\,\text{div}\mathbf{E} = 0, \tag{6}$$

where $k_0 = \omega/c$ is the magnitude of the wave vector $\mathbf{k}_0$ of the incident field in vacuum, and define the complex current density

$$\mathbf{J} = -i\frac{\omega}{4\pi}\hat{\varepsilon}\,\mathbf{E}, \quad \text{div}\,\mathbf{J} = 0. \tag{7}$$

The first Eq. (7) reduces in the static limit ($\omega \to 0$) to Ohm's law, given by the second Eq. (4).

III. COMPACT GROUP APPROACH TO HOMOGENIZATION OF CONDUCTING SYSTEMS

The main points of this approach in application to macroscopically homogeneous and isotropic nonconducting systems are discussed in detail in Refs. [48–51]. Here, closely following the summary in Ref. [51], we outline a generalization of the approach to macroscopically homogeneous and isotropic dispersions $\mathcal{D}$ comprising conducting constituents, such as conducting dielectrics or imperfectly insulating materials. In view of the Kramers-Kronig relations in the linear

response theory, we assume that for a given $\mathcal{D}$, the complex permittivities of all the constituents have structure (5), where ε and σ are in general piecewise-continuous and bounded real functions of spacial coordinates; and that its $\hat{\varepsilon}_{\text{eff}} = \varepsilon_{\text{eff}} + i4\pi\sigma_{\text{eff}}/\omega$ can be calculated based upon the following suggestions:

(1) $\mathcal{D}$ is equivalent, in its response to a long-wavelength probing field ($\omega \to 0$), to an auxiliary system $\mathcal{S}$ prepared by embedding the constituents (particles and matrix) of $\mathcal{D}$ into a uniform host (perhaps, imagined) $\mathcal{M}$ with some permittivity $\hat{\varepsilon}_{\text{f}}$.

(2) $\mathcal{S}$ can be viewed as a set of compact groups of both particles and regions occupied by the real matrix. The compact groups are defined as macroscopic regions whose typical sizes d are much smaller than the wavelength λ of probing radiation in $\mathcal{M}$, but which yet include sufficiently large numbers N of particles to remain macroscopic and retain the properties of the entire $\mathcal{S}$.

(3) The complex permittivity distribution in $\mathcal{S}$ is

$$\hat{\varepsilon}(\mathbf{r}) = \hat{\varepsilon}_{\text{f}} + \delta\hat{\varepsilon}(\mathbf{r}), \tag{8}$$

where $\delta\hat{\varepsilon}(\mathbf{r})$ is the contribution from a compact group located at point $\mathbf{r}$. The explicit form of $\delta\hat{\varepsilon}(\mathbf{r})$ is modeled according to the geometrical and electrical parameters of $\mathcal{D}$'s constituents.

(4) $\hat{\varepsilon}_{\text{eff}}$ can be found as the proportionality coefficient in the relation

$$\langle\mathbf{J}(\mathbf{r})\rangle = -i\frac{\omega}{4\pi}\langle\hat{\varepsilon}(\mathbf{r})\mathbf{E}(\mathbf{r})\rangle = -i\frac{\omega}{4\pi}\hat{\varepsilon}_{\text{eff}}\langle\mathbf{E}(\mathbf{r})\rangle, \tag{9}$$

where $\mathbf{J}(\mathbf{r})$ and $\mathbf{E}(\mathbf{r})$ are the local values of the complex current and electric field, respectively, and the angle brackets stand for the ensemble averaging. In the static limit, provided $\lim_{\omega\to 0}\omega\varepsilon(\mathbf{r}) = 0$ and $\mathbf{E}(\mathbf{r})$ is real-valued, Eq. (9) reduces to the common definition [17,18,20] of the effective conductivity:

$$\langle\mathbf{j}(\mathbf{r})\rangle = \langle\sigma(\mathbf{r})\mathbf{E}(\mathbf{r})\rangle = \sigma_{\text{eff}}\langle\mathbf{E}(\mathbf{r})\rangle. \tag{10}$$

(5) The electric field distribution $\mathbf{E}(\mathbf{r})$ in $\mathcal{S}$ obeys the equation

$$\Delta\mathbf{E} + k_0^2\hat{\varepsilon}_{\text{f}}\mathbf{E} - \text{grad}\,\text{div}\mathbf{E} = -k_0^2\delta\hat{\varepsilon}\mathbf{E}, \tag{11}$$

which directly follows from Eqs. (6) and (8). The equivalent integral equation is

$$\mathbf{E}(\mathbf{r}) = \mathbf{E}_0(\mathbf{r}) - \int_V d\mathbf{r}'\,\text{T}(|\mathbf{r} - \mathbf{r}'|)k_0^2\delta\hat{\varepsilon}(\mathbf{r}')\mathbf{E}(\mathbf{r}'), \tag{12}$$

where $\mathbf{E}_0(\mathbf{r}) = \mathbf{E}_0\exp(i\mathbf{k}\cdot\mathbf{r})$, $\mathbf{E}_0$, and $\mathbf{k} = \hat{\varepsilon}_{\text{f}}^{1/2}\mathbf{k}_0$ (with $\text{Im}\,\hat{\varepsilon}_{\text{f}}^{1/2} \geqslant 0$) are, respectively, the incident wave field, its amplitude, and its wave vector in $\mathcal{M}$, and $\text{T}(r)$ is the Green's tensor of Eq. (11).

(6) The formal solution for $\mathbf{E}(\mathbf{r})$ and those for $\mathbf{J}(\mathbf{r})$, $\langle\mathbf{E}(\mathbf{r})\rangle$, and $\langle\mathbf{J}(\mathbf{r})\rangle$ are representable in the form of infinite iterative series. For systems whose constituents have the permittivities of form (5), the functions $k_0^2\delta\hat{\varepsilon}(\mathbf{r})$ in the integrands and also the function $\omega\hat{\varepsilon}(\mathbf{r})$ remain bounded even at $\omega \to 0$, where $|\mathbf{k}| \to 0$ as well. Mathematically, the situation is identical to that for nonconducting systems and can be treated analogously. Namely, in the iterative series for $\langle\mathbf{E}(\mathbf{r})\rangle$ and $\langle\mathbf{J}(\mathbf{r})\rangle$, each T under the integral sign is replaced by its decomposition $\widetilde{\text{T}}$, derived for a spherical exclusion volume of radius $a \to 0$,

into a Dirac δ-function singular part and a principal value part [56,57]:

$$\widetilde{T}_{\alpha\beta}(\mathbf{r}) = \frac{1}{3k^2}\delta_{\alpha\beta}\delta(\mathbf{r})\,e^{ikr} + \frac{1}{4\pi k^2}\left(\frac{1}{r^3} - \frac{ik}{r^2}\right)$$

$$\times (\delta_{\alpha\beta} - 3e_\alpha e_\beta)\,e^{ikr} - \frac{1}{4\pi r}(\delta_{\alpha\beta} - e_\alpha e_\beta)\,e^{ikr}, \quad (13)$$

where $\delta(\mathbf{r})$ is the Dirac δ function, $\delta_{\alpha\beta}$ is the Kronecker delta, and e_α is the α-component of the unit vector $\mathbf{e} = \mathbf{r}/r$. The contributions to $\langle\mathbf{E}(\mathbf{r})\rangle$ made by the subseries containing, in their integrands, the principal value parts are estimated to be of the order $|\hat{\varepsilon}_f|k_0^2 L^3/d$, at most [48], as compared to those made by the subseries with only the Dirac δ-function parts. For a finite typical linear size L of the system, the former can be decreased below any preset value by taking a sufficiently small k_0. So, passing to the limit $\omega \to 0$ and formally replacing each $\widetilde{T}$ in the integrals for $\langle\mathbf{E}(\mathbf{r})\rangle$ and $\langle\mathbf{J}(\mathbf{r})\rangle$ by its δ-function part, we obtain

$$\lim_{\omega\to 0}\langle\mathbf{E}(\mathbf{r})\rangle = \lim_{\omega\to 0}[1 + \langle\hat{Q}(\mathbf{r})\rangle]\mathbf{E}_0, \quad (14)$$

$$\lim_{\omega\to 0}\langle\mathbf{J}(\mathbf{r})\rangle = -i\lim_{\omega\to 0}\frac{\omega\hat{\varepsilon}_f}{4\pi}[1 - 2\langle\hat{Q}(\mathbf{r})\rangle]\mathbf{E}_0, \quad (15)$$

where

$$\hat{Q}(\mathbf{r}) \equiv \sum_{s=1}^{\infty}\left(-\frac{1}{3\hat{\varepsilon}_f}\right)^s (\delta\hat{\varepsilon}(\mathbf{r}))^s. \quad (16)$$

(7) The above results can be obtained without resort to iterative series. Indeed, it follows from Eq. (13) that

$$\lim_{\omega\to 0} k_0^2\hat{\varepsilon}_f\widetilde{T}_{\alpha\beta}(\mathbf{r}) = \tau_{\alpha\beta}^{(1)} + \tau_{\alpha\beta}^{(2)}, \quad (17)$$

where

$$\tau_{\alpha\beta}^{(1)} = \frac{1}{3}\,\delta_{\alpha\beta}\delta(\mathbf{r}), \quad \tau_{\alpha\beta}^{(2)} = \frac{\delta_{\alpha\beta} - 3e_\alpha e_\beta}{4\pi r^3}. \quad (18)$$

Substituting Eqs. (17) and (18) into Eq. (12), making simple algebraic manipulations and statistical averaging, and implying that $\omega \to 0$, we obtain

$$\langle\mathbf{E}(\mathbf{r})\rangle = \left\langle\frac{3\hat{\varepsilon}_f}{3\hat{\varepsilon}_f + \delta\hat{\varepsilon}(\mathbf{r})}\right\rangle\mathbf{E}_0 - 3\int_V d\mathbf{r}'\tau^{(2)}(|\mathbf{r}-\mathbf{r}'|)$$

$$\times \left\langle\frac{\delta\hat{\varepsilon}(\mathbf{r}')}{3\hat{\varepsilon}_f + \delta\hat{\varepsilon}(\mathbf{r})}\mathbf{E}(\mathbf{r}')\right\rangle, \quad (19)$$

$$\langle\mathbf{J}(\mathbf{r})\rangle = -i\frac{\omega}{4\pi}\hat{\varepsilon}_f\left[1 + 2\left\langle\frac{\delta\hat{\varepsilon}(\mathbf{r})}{3\hat{\varepsilon}_f + \delta\hat{\varepsilon}(\mathbf{r})}\right\rangle\right]\mathbf{E}_0 + i\frac{3}{4\pi}$$

$$\times \int_V d\mathbf{r}'\tau^{(2)}(|\mathbf{r}-\mathbf{r}'|)\left\langle\frac{\omega\,\hat{\varepsilon}(\mathbf{r})\,\delta\hat{\varepsilon}(\mathbf{r}')}{3\hat{\varepsilon}_f + \delta\hat{\varepsilon}(\mathbf{r})}\mathbf{E}(\mathbf{r}')\right\rangle. \quad (20)$$

For macroscopically isotropic and homogeneous systems, two-point statistical averages depend only on $|\mathbf{r}-\mathbf{r}'|$. Due to this symmetry and because of a special form of the angular dependence of $\tau_{\alpha\beta}^{(2)}$, the integrals in Eqs. (19) and (20) vanish. Finally, viewing the expressions in the angle brackets as the sums of infinite series in $\delta\hat{\varepsilon}(\mathbf{r})$, we arrive at Eqs. (14)–(16).

This consideration is very similar to that used in the strong-property-fluctuation theory (SPFT) [19,56,58–64]. However, our theory gives another interpretation to $\delta\hat{\varepsilon}(\mathbf{r})$, appeals to the macroscopic symmetry of the entire system instead of the

symmetry of correlation functions, and postulates no condition on the stochastic field $\hat{\xi}(\mathbf{r}) = [\hat{\varepsilon}(\mathbf{r}) - \hat{\varepsilon}_f]/[2\hat{\varepsilon}_f + \hat{\varepsilon}(\mathbf{r})] = \delta\hat{\varepsilon}(\mathbf{r})/[3\hat{\varepsilon}_f + \delta\hat{\varepsilon}(\mathbf{r})]$ in order to improve the convergence of the iteration procedure and decide on the value of $\hat{\varepsilon}_f$. Once the latter is determined, the analysis of $\hat{\varepsilon}_{eff}$ reduces to modeling $\delta\hat{\varepsilon}(\mathbf{r})$, calculating its moments $\langle(\delta\hat{\varepsilon}(\mathbf{r}))^s\rangle$, and finding their sum in Eqs. (14) and (15).

IV. DETERMINATION OF $\hat{\varepsilon}_f$

If the permittivities of the constituents, that of $\mathcal{M}$, and $\hat{\varepsilon}_{eff}$ have at $\omega \to 0$ the structure (5), then, at least in this limit, it is the Bruggeman-type of homogenization $\hat{\varepsilon}_f = \hat{\varepsilon}_{eff}$ that is compatible with the formalism of the CGA and definition (9). To prove this statement, we first remind that $\mathbf{E}_0$ is the amplitude of the probing electric field in the uniform fictitious matrix of permittivity $\hat{\varepsilon}_f$, and $\langle\mathbf{E}(\mathbf{r})\rangle$ is the effective electric field in the homogenized dispersion of permittivity $\hat{\varepsilon}_{eff}$, caused by the same probing field. Next, we recall the boundary condition [55]

$$\hat{\varepsilon}_1 E_{1n} = \hat{\varepsilon}_2 E_{2n}$$

for the normal components of complex electric fields at the surface between two conducting dielectrics (or imperfectly insulating materials) with permittivities of type (5). For the surface between the fictitious matrix and the homogenized dispersion, it gives

$$\hat{\varepsilon}_f \mathbf{E}_{0n} = \hat{\varepsilon}_{eff}\langle\mathbf{E}(\mathbf{r})\rangle_n. \quad (21)$$

This relation, Eq. (9), and Eqs. (14)–(16) yield, at $\omega \to 0$, the system of equations

$$\hat{\varepsilon}_f = \hat{\varepsilon}_{eff}(1 + \langle\hat{Q}\rangle),$$
$$\hat{\varepsilon}_f(1 - 2\langle\hat{Q}\rangle) = \hat{\varepsilon}_{eff}(1 + \langle\hat{Q}\rangle). \quad (22)$$

Since $\hat{\varepsilon}_f \neq 0$, it follows immediately that

$$\hat{\varepsilon}_f = \hat{\varepsilon}_{eff} \quad (23)$$

and, for this $\hat{\varepsilon}_f$,

$$\langle\hat{Q}(\mathbf{r})\rangle = 0. \quad (24)$$

The latter is the desired governing equation for $\hat{\varepsilon}_{eff}$. It is valid in the limit $\omega \to 0$.

It can be shown [51] that for two-constituent systems (say, hard spheres embedded in a uniform host), Eqs. (23) and (24) reproduce the Bruggeman result [14,15,65] derived within the assumption that spherical inclusions of all constituent materials are placed in the effective medium. The same Eqs. (23), (24), and Bruggeman result also follow, in the quasistatic limit, from the SPFT [60] for hard spheres where the condition $\langle\hat{\xi}(\mathbf{r})\rangle = 0$ is imposed to eliminate the secular terms and the bilocal approximation is implemented for a special case of the spherically symmetric two-point correlation function $\langle\hat{\xi}(\mathbf{r})\hat{\xi}(\mathbf{r}')\rangle$.

V. STATISTICAL MOMENTS $\langle[\delta\hat{\varepsilon}(\mathbf{r})]^s\rangle$

We consider a dispersion of N spherically symmetrical core-shell particles embedded into a uniform matrix. Suppose

that the local permittivity value at a point $\mathbf{r}$ within the dispersion is determined by the distance $l \equiv \min\limits_{1 \leqslant a \leqslant N} |\mathbf{r} - \mathbf{r}_a|$ from $\mathbf{r}$ to the center of the nearest ball as

$$\hat{\varepsilon}(\mathbf{r}) = \begin{cases} \hat{\varepsilon}_1 & \text{if} \quad l < R_1, \\ \hat{\varepsilon}_2 & \text{if} \quad R_1 < l < R_2, \\ \hat{\varepsilon}_0 & \text{if} \quad l > R_2. \end{cases} \quad (25)$$

Here R_1 is the radius of the core of complex permittivity $\hat{\varepsilon}_1$, R_2 is the outer radius of the shell of complex permittivity $\hat{\varepsilon}_2$, and $\hat{\varepsilon}_0$ is the complex permittivity of the matrix. Within the CGA [48–51], such a system can be modelled as follows.

Let $\theta(x)$ be the Heaviside step function and $\chi_a^{(q)}(\mathbf{r}) = \theta(R_q - |\mathbf{r} - \mathbf{r}_a|)$ ($q = 0, 1, 2$) be the characteristic functions of balls centered at point $\mathbf{r}_a$ and having radii R_q. Suggesting that $R_1 < R_2 < R_0$ and allowing the balls to overlap, consider the complex permittivity distribution of form (8) with

$$\delta\hat{\varepsilon}(\mathbf{r}) = \Pi_1(\mathbf{r})\Delta\hat{\varepsilon}_1 + [\Pi_2(\mathbf{r}) - \Pi_1(\mathbf{r})]\Delta\hat{\varepsilon}_2$$
$$+ [\Pi_0(\mathbf{r}) - \Pi_2(\mathbf{r})]\Delta\hat{\varepsilon}_0, \quad (26)$$

where $\Delta\hat{\varepsilon}_q = \hat{\varepsilon}_q - \hat{\varepsilon}_{\text{f}}$, and each

$$\Pi_q(\mathbf{r}) = 1 - \prod_{a=1}^{N} \left[1 - \chi_a^{(q)}(\mathbf{r})\right] \quad (27)$$

is the characteristic (indicator) function of the collection of balls of radius R_q. In the limit $R_0 \to \infty$, $\Pi_0(\mathbf{r}) \to 1$ and Eq. (26) leads to the model permittivity distribution (25) for a dispersion of penetrable core-shell particles embedded into a uniform matrix of permittivity $\hat{\varepsilon}_0$. Note that R_0 is a convenient auxiliary parameter (having nothing to do with the physical geometry) which is used for the host matrix to be introduced within the same formal algorithm as the other constituents are. The characteristic function of the entire region occupied by the substance of permittivity $\mathcal{E}_q$ in this dispersion is given by the coefficient function in front of the corresponding $\Delta\hat{\varepsilon}_q$. It is readily verified that the characteristic functions of regions with different permittivities are mutually orthogonal.

Further, we limit ourselves to the case of particles with hard cores. Then $\chi_a^{(1)}(\mathbf{r})\chi_b^{(1)}(\mathbf{r}) = \delta_{ab}\chi_a^{(1)}(\mathbf{r})$, where δ_{ab} is the Kronecker delta, and $\Pi_1(\mathbf{r})$ reduces to

$$\Pi_1(\mathbf{r}) = \sum_{a=1}^{N} \chi_a^{(1)}(\mathbf{r}), \quad (28)$$

with the additional restriction $|\mathbf{r}_a - \mathbf{r}_b| \geqslant 2R_1$ on the locations of any two balls.

For a macroscopically homogeneous and isotropic system

$$\left\langle \sum_{a=1}^{N} \chi_a^{(1)}(\mathbf{r}) \right\rangle = c,$$

where c is the volume concentration of the hard cores. In view of this fact and the mutual orthogonality of the characteristic functions of regions with different permittivities, the moments of the function (26) can be represented in the limit $R_0 \to \infty$ as

$$\langle [\delta\hat{\varepsilon}(\mathbf{r})]^s \rangle = c(\Delta\hat{\varepsilon}_1)^s + [\phi(c, \delta) - c](\Delta\hat{\varepsilon}_2)^s$$
$$+ [1 - \phi(c, \delta)](\Delta\hat{\varepsilon}_0)^s, \quad (29)$$

where

$$\phi(c, \delta) \equiv \langle \Pi_2(\mathbf{r}) \rangle = \left\langle \left[1 - \prod_{a=1}^{N} \left(1 - \chi_a^{(2)}(\mathbf{r})\right)\right] \right\rangle$$

$$= \left\langle \sum_{1 \leqslant a \leqslant N} \chi_a^{(2)}(\mathbf{r}) - \sum_{1 \leqslant a < b \leqslant N} \chi_a^{(2)}(\mathbf{r})\chi_b^{(2)}(\mathbf{r}) \right.$$

$$\left. + \sum_{1 \leqslant a < b < c \leqslant N} \chi_a^{(2)}(\mathbf{r})\chi_b^{(2)}(\mathbf{r})\chi_c^{(2)}(\mathbf{r}) - \ldots \right\rangle \quad (30)$$

is the effective volume concentration of hard-core–penetrable-shell particles [20]. Besides c, it depends on the relative thickness of the shell $\delta = (R_2 - R_1)/R_1$; in particular, $\phi(c, 0) = c$. The averaged values of the sums in Eq. (30) are calculated using the partial distribution functions $F_s(\mathbf{r}_1, \mathbf{r}_2, \ldots, \mathbf{r}_s)$ for the system under consideration.

For hard-core–hard-shell particles Eq. (30) gives

$$\phi(c, \delta) = c(1 + \delta)^3. \quad (31)$$

VI. THE CASE OF INHOMOGENEOUS ISOTROPIC SHELLS

To extend the results of Sec. V to dispersions of spherically symmetrical particles with hard cores and adjacent inhomogeneous penetrable shells, we begin with the situation where each shell consists of M concentric spherical layers with outer radii $R_{2,m}$ (grouped in the order of increasing magnitude) and constant dielectric permittivities $\hat{\varepsilon}_{2,m}$, $m = 1, 2, \ldots, M$. Next, we suggest that the local permittivity distribution within the dispersion is given by this law, generalizing Eq. (25):

$$\hat{\varepsilon}(\mathbf{r}) = \begin{cases} \hat{\varepsilon}_1 & \text{if} \quad l < R_1, \\ \hat{\varepsilon}_{2,1} & \text{if} \quad R_1 < l < R_{2,1}, \\ \hat{\varepsilon}_{2,m} & \text{if} \quad R_{2,m-1} < l < R_{2,m}, \ 2 \leqslant m \leqslant M, \\ \hat{\varepsilon}_0 & \text{if} \quad l > R_{2,M}. \end{cases} \quad (32)$$

Let $\chi_a^{(2,m)}(\mathbf{r}) = \theta(R_{2,m} - |\mathbf{r} - \mathbf{r}_a|)$ be the characteristic functions of balls centered at point $\mathbf{r}_a$, having radii $R_{2,m}$, and allowed to overlap. Then the characteristic functions of the collections of balls with radii $R_{2,m}$ are

$$\Pi_{2,m}(\mathbf{r}) = 1 - \prod_{a=1}^{N} \left[1 - \chi_a^{(2,m)}(\mathbf{r})\right]. \quad (33)$$

Repeating almost literally the reasoning in Sec. V, we can represent the distribution (32) in form (8) with

$$\delta\hat{\varepsilon}(\mathbf{r}) = [1 - \Pi_{2,M}(\mathbf{r})]\Delta\hat{\varepsilon}_0 + \Pi_1(\mathbf{r})\Delta\hat{\varepsilon}_1$$
$$+ [\Pi_{2,1}(\mathbf{r}) - \Pi_1(\mathbf{r})]\Delta\hat{\varepsilon}_{2,1}$$
$$+ \sum_{m=2}^{M} [\Pi_{2,m}(\mathbf{r}) - \Pi_{2,m-1}(\mathbf{r})]\Delta\hat{\varepsilon}_{2,m}, \quad (34)$$

where $\Delta\hat{\varepsilon}_{2,m} = \hat{\varepsilon}_{2,m} - \hat{\varepsilon}_{\text{f}}$. Correspondingly,

$$\langle [\delta\hat{\varepsilon}(\mathbf{r})]^s \rangle = [1 - \phi(c, \delta_M)](\Delta\hat{\varepsilon}_0)^s + c(\Delta\hat{\varepsilon}_1)^s$$
$$+ \sum_{m=1}^{M} [\phi(c, \delta_m) - \phi(c, \delta_{m-1})](\Delta\hat{\varepsilon}_{2,m})^s, \quad (35)$$

where $\delta_m = (R_{2,m} - R_1)/R_1$, $\phi(c, \delta_m) \equiv \langle \Pi_{2,m}(\mathbf{r}) \rangle$ is given by Eq. (30) at $\delta = \delta_m$, and we denoted $\delta_0 = 0$. Finally, passing to the limits $M \to \infty$, $|\delta_m - \delta_{m-1}| \to 0$ ($\delta_M = \text{const}$) and assuming $\phi(c, \delta)$ to be differentiable with respect to δ, for a dispersion of particles with a piecewise-continuous complex permittivity profile $\hat{\varepsilon}_2(r)$ of the shells, we obtain

$$\langle [\delta \hat{\varepsilon}(\mathbf{r})]^s \rangle = [1 - \phi(c, \delta_M)](\Delta \hat{\varepsilon}_0)^s + c(\Delta \hat{\varepsilon}_1)^s$$
$$+ \int_0^{\delta_M} \frac{\partial \phi(c, u)}{\partial u} [\Delta \hat{\varepsilon}_2(u)]^s du, \quad (36)$$

where $\Delta \hat{\varepsilon}_2(u)$ is the deviation $\hat{\varepsilon}_2(r) - \hat{\varepsilon}_f$ as a function of $u = (r - R_1)/R_1$ and δ_M corresponds to the outermost edge of the shell.

For a uniform shell ($\Delta \hat{\varepsilon}_2 = \text{const}$), Eq. (36) immediately reduces to Eq. (29) with $\delta = \delta_M = \delta_1$.

VII. EQUATIONS FOR EFFECTIVE CONDUCTIVITY

In the case of uniform shells, where the moments $\langle [\delta \hat{\varepsilon}(\mathbf{r})]^s \rangle$ are given by Eq. (29), the sums involved in Eq. (24) take the form $\sum_{s=1}^{\infty} (-\Delta \hat{\varepsilon}_q / 3 \hat{\varepsilon}_{\text{eff}})^s$. For $|\Delta \hat{\varepsilon}_q / 3 \hat{\varepsilon}_{\text{eff}}| < 1$, they reduce to infinite geometric series, so

$$\sum_{s=1}^{\infty} \left(-\frac{\Delta \hat{\varepsilon}_q}{3 \hat{\varepsilon}_{\text{eff}}} \right)^s = -\frac{\hat{\varepsilon}_q - \hat{\varepsilon}_{\text{eff}}}{2 \hat{\varepsilon}_{\text{eff}} + \hat{\varepsilon}_q}. \quad (37)$$

For $|\Delta \hat{\varepsilon}_q / 3 \hat{\varepsilon}_{\text{eff}}| \geqslant 1$, the left-hand side in Eq. (37) can be treated, as was shown in Sec. III, as an asymptotic series of the right-hand side, so that the restriction $|\Delta \hat{\varepsilon}_q / 3 \hat{\varepsilon}_{\text{eff}}| < 1$ can be omitted. The resulting equation for $\hat{\varepsilon}_{\text{eff}}$ is

$$[1 - \phi(c, \delta)] \frac{\hat{\varepsilon}_0 - \hat{\varepsilon}_{\text{eff}}}{2 \hat{\varepsilon}_{\text{eff}} + \hat{\varepsilon}_0} + c \frac{\hat{\varepsilon}_1 - \hat{\varepsilon}_{\text{eff}}}{2 \hat{\varepsilon}_{\text{eff}} + \hat{\varepsilon}_1}$$
$$+ [\phi(c, \delta) - c] \frac{\hat{\varepsilon}_2 - \hat{\varepsilon}_{\text{eff}}}{2 \hat{\varepsilon}_{\text{eff}} + \hat{\varepsilon}_2} = 0. \quad (38)$$

To extract the equation for the quasistatic σ_{eff}, we pass in Eq. (38) to the limit $\omega \to 0$ and assume that

$$2\sigma_{\text{eff}} + \sigma_q \gg \frac{\omega}{4\pi} (2\varepsilon_{\text{eff}} + \varepsilon_q),$$
$$|\sigma_q - \sigma_{\text{eff}}| \gg \frac{\omega}{4\pi} |\varepsilon_q - \varepsilon_{\text{eff}}|. \quad (39)$$

Then, retaining the first term in the formal perturbation series in ω for the left-hand side of Eq. (38), we obtain

$$[1 - \phi(c, \delta)] \frac{\sigma_0 - \sigma_{\text{eff}}}{2 \sigma_{\text{eff}} + \sigma_0} + c \frac{\sigma_1 - \sigma_{\text{eff}}}{2 \sigma_{\text{eff}} + \sigma_1}$$
$$+ [\phi(c, \delta) - c] \frac{\sigma_2 - \sigma_{\text{eff}}}{2 \sigma_{\text{eff}} + \sigma_2} = 0. \quad (40)$$

In view of Eq. (39), the sufficient condition for the validity of Eq. (40) can be represented as

$$|\sigma_{\text{eff}} - \sigma_q| \gg \frac{\omega}{4\pi} (2\varepsilon_{\text{eff}} + \varepsilon_q), \quad q = 1, 2, 3. \quad (41)$$

The generalizations of Eqs. (38) and (40) to dispersions of particles with inhomogeneous isotropic shells are evident [see Eq. (36)]:

$$[1 - \phi(c, \delta_M)] \frac{\hat{\varepsilon}_0 - \hat{\varepsilon}_{\text{eff}}}{2 \hat{\varepsilon}_{\text{eff}} + \hat{\varepsilon}_0} + c \frac{\hat{\varepsilon}_1 - \hat{\varepsilon}_{\text{eff}}}{2 \hat{\varepsilon}_{\text{eff}} + \hat{\varepsilon}_1}$$
$$+ \int_0^{\delta_M} \frac{\partial \phi(c, u)}{\partial u} \frac{\hat{\varepsilon}_2(u) - \hat{\varepsilon}_{\text{eff}}}{2 \hat{\varepsilon}_{\text{eff}} + \hat{\varepsilon}_2(u)} du = 0, \quad (42)$$
$$[1 - \phi(c, \delta_M)] \frac{\sigma_0 - \sigma_{\text{eff}}}{2 \sigma_{\text{eff}} + \sigma_0} + c \frac{\sigma_1 - \sigma_{\text{eff}}}{2 \sigma_{\text{eff}} + \sigma_1}$$
$$+ \int_0^{\delta_M} \frac{\partial \phi(c, u)}{\partial u} \frac{\sigma_2(u) - \sigma_{\text{eff}}}{2 \sigma_{\text{eff}} + \sigma_2(u)} du = 0. \quad (43)$$

Based upon the volume averaging procedure, Eqs. (38) and (40) were first proposed in Ref. [66], and Eqs. (42) and (43) in Ref. [67]. Here, Eqs. (40) and (43) are finally substantiated with a statistical mechanics formalism and an internally closed homogenization procedure.

Note that care must be taken when applying Eqs. (40) and (43) to experimental data. In practice, σ_{eff} is often identified with the quasistatic conductivity recovered from impedance measurements at very small (say, $\omega/2\pi \leqslant 1$ kHz), yet nonzero frequencies. Equations (40) and (43) remain applicable to such situations as long as all inequalities (39) hold true for the real and imaginary parts of the quasistatic complex permittivities of the constituents.

We complete this section by mentioning that various mixing rules of the Maxwell-Garnett type are formally obtainable within the CGA by setting $\hat{\varepsilon}_f = \hat{\varepsilon}_0$ [48–51]. Then the moments (36) take the form

$$\langle [\delta \hat{\varepsilon}(\mathbf{r})]^s \rangle = c(\hat{\varepsilon}_1 - \hat{\varepsilon}_0)^s + \int_0^{\delta_M} \frac{\partial \phi(c, u)}{\partial u} [\hat{\varepsilon}_2(u) - \hat{\varepsilon}_0]^s du$$

to eventually give, in the quasistatic limit,

$$\sigma_{\text{eff}} = \sigma_0 \frac{1 + 2F}{1 - F}, \quad (44)$$

where

$$F = c \frac{\sigma_1 - \sigma_0}{2\sigma_0 + \sigma_1} + \int_0^{\delta_M} \frac{\partial \phi(c, u)}{\partial u} \frac{\sigma_2(u) - \sigma_0}{2\sigma_0 + \sigma_2(u)} du.$$

For the shells consisting of M concentric spherical layers with constant conductivities $\sigma_{2,m}$, the last integral equals

$$\sum_{m=1}^{M} [\phi(c, \delta_m) - \phi(c, \delta_{m-1})] \frac{\sigma_{2,m} - \sigma_0}{2\sigma_0 + \sigma_{2,m}}.$$

VIII. COMPARISON WITH ANALYTICAL RESULTS AND NUMERICAL SIMULATIONS

Before we proceed to processing experimental data with the above theory, it is of crucial importance to test its validity by contrasting it with other authors' analytical and computer simulation results.

For 3D systems of particles with hard cores and fully penetrable shells calculations [52], done within the

TABLE I. Electrical parameters, in S/cm, used in simulations [44,46] (shells with constant conductivity) and [45] [shells with inhomogeneous conductivity profiles (51)].

Simulations	σ_0	σ_1	σ_2	σ'_{min}	σ'_{max}
[44,46]	1×10^{-8}	1×10^{-12}	1×10^{-4}		
[45]	1×10^{-8}	1×10^{-12}		1×10^{-6}	1×10^{-4}

scaled-particle approximation [68] for hard-sphere fluids, give

$$\phi(c, \delta) = 1 - (1 - c) \exp\left[-\frac{((1 + \delta)^3 - 1)c}{1 - c}\right]$$
$$\times \exp\left\{-\frac{3(1 + \delta)^3 c^2}{2(1 - c)^3}\left[2 - \frac{3}{1 + \delta} + \frac{1}{(1 + \delta)^3}\right.\right.$$
$$\left.\left. - \left(\frac{3}{1 + \delta} - \frac{6}{(1 + \delta)^2} + \frac{3}{(1 + \delta)^3}\right)c\right]\right\}. \quad (45)$$

This result is in very good agreement with Monte Carlo simulations [53] (see also Ref. [54]). Simulation results for σ_{eff} [and $\phi(c, \delta)$] of 3D systems of monosized particles are available in [44–46], where σ_{eff} was calculated using the RRN approach [69,70].

In simulations [44–46], the virtual RRN samples, representing the morphology and phase structure of simulated dispersions, were built from a matrix with 300^3 cubic cells by placing spherical grains randomly into the matrix and using a special algorithm for avoiding conflicts of spatial restrictions on the grain locations. Each cell was marked as belonging to a grain if the center of the cell lay inside it. The procedure was repeated until the assumed volume fraction c of the filler was attained. The residual part of the virtual sample (not belonging to the grains) was attributed to either the shells, with prescribed thickness t, or the matrix (all cells belonging to neither the grains nor the shell). Finally, each cell was represented as a parallel combination of a resistor and a capacitor, with their parameters taken according to the assumed material parameters of all the phases; the electrical parameters used are summarized in Table I. Replacing each pair of neighboring cells by an equivalent electrical circuit with the corresponding impedance and the nodes at the centers of the cells, the virtual samples were analyzed as 3D networks of such impedances.

We use results [44–46,52] to test the validity of Eqs. (40) and (43) in the following five steps.

A. Mapping the geometrical parameters in models [46,52] onto each other

This step is to contrast results [46,52] for $\phi(c, \delta)$ in order to find the relations between the parameters c and δ for a dispersion of spherical core-shell particles [52] and their counterparts c' and δ' in simulations [44–46].

Evidently, for a given t and under the condition that the assumed volume fraction c of the filler is attained, $c' = c$, the simulation procedure [46] leads to values of δ' different from those of δ. Indeed, suppose that N spherical grains of radius $a/2$, where a is the edge of the cubic cell, are used to generate a virtual sample of volume V. Then $c' = Na^3/V$ and
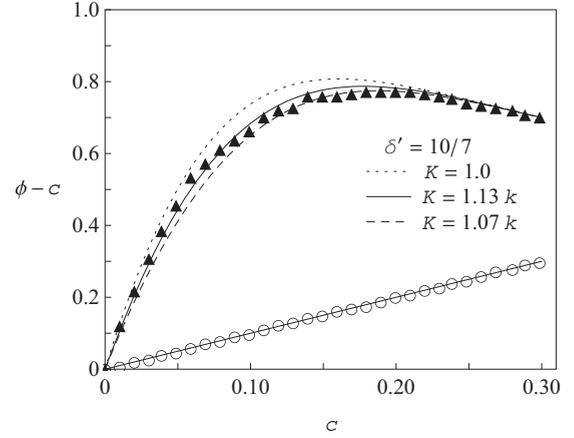

FIG. 2. Simulation data [46] for the volume concentration ($\phi - c$, ▲) of freely penetrable shells of thickness $t = 5\,\mu$m as a function of the assumed volume concentration (c, ○) of hard grains of diameter $d = 7\,\mu$m, and the fits to these data with Eq. (45) for different values of the mapping parameter K in Eq. (46).

$\delta' = 2t/a$, for only one cell can belong to each grain. To achieve this filler concentration in the same-volume dispersion of N spherical particles with shell thickness t, their core radius must be equal to $(4\pi/3)^{-1/3}a$. For such particles, the relative shell thickness $\delta = (4\pi/3)^{1/3}t/a$. Correspondingly,

$$\delta = K\delta', \quad (46)$$

where, in our example, $K = k \equiv (\pi/6)^{1/3} \approx 0.806$. Considering K as a fitting parameter, one can generalize Eq. (46) to the situations where each grain contains a large number of cells. The greater this number is, the closer to unity K is expected to be. However, for $a = 0.5\,\mu$m, used in Refs. [44–46], the deviation of K from unity should be noticeable.

The results of applying Eqs. (45) and (46) to simulation data [46] for the composition of dispersions of spherical hard-core–penetrable-shell particles at different values of c are presented in Figs. 2 and 3. They clearly demonstrate that under the proper choice of K, these equations describe data [46] very well; the found values of K turn out to be close to our above estimates.
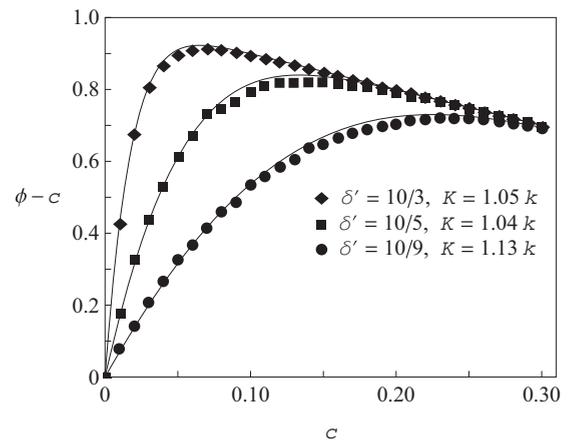

FIG. 3. Simulation data [46] and the fits analogous to those in Fig 2, but for $d = 3$ (♦), 5 (■), and 9 μm (●) at fixed $t = 5\,\mu$m.
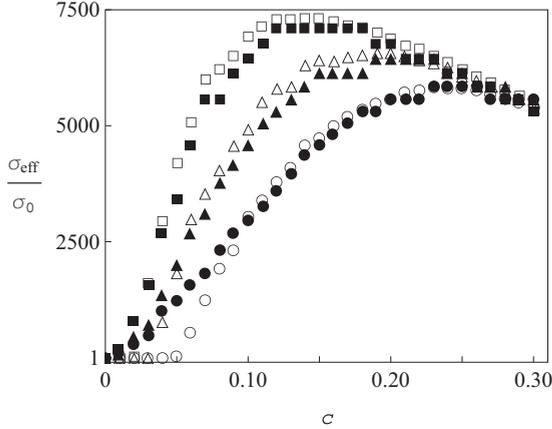
FIG. 4. Simulation data [46] for σ_{eff} as a function of c for a fixed shell thickness $t = 5\,\mu\text{m}$ and grain diameters $d = 5$ (■), 7 (▲), and $9\,\mu\text{m}$ (●). Empty markers (□, △, and ○): our corresponding results obtained from Eq. (40) by setting ϕ equal to the simulated values [46], shown in Figs. 2 and 3.

B. Verifying functional relationship (40) between σ_{eff} and ϕ

With this object in view, the dispersion composition is assumed to be known for different values of c at fixed t and d. Taking the corresponding values of ϕ from simulations [46] (Figs. 2 and 3), we then use Eq. (40) to calculate σ_{eff} as a function of c for given t and d without referring to Eqs. (45) and (46).

The results so obtained are shown in Fig. 4, together with conductivity simulation results [46]. If $c \gtrsim 0.07$, then the agreement between both theories is good for all three sets of data ($d = 5, 7$, and $9\,\mu\text{m}$ at fixed $t = 5\,\mu\text{m}$). At lower values of c, our theory predicts the percolation-type behavior of σ_{eff} (see also Fig. 5 and the inset), with the threshold concentration c_{c} that can be estimated from the relation $\phi = 1/3$ [66]. For the indicated sets of data, the estimations with Eqs. (40) and (46) give, respectively, $c_{\text{c}} = 0.020$ ($K/k = 1.04$, $d = 5\,\mu\text{m}$), 0.034 ($K/k = 1.07$, $d = 7\,\mu\text{m}$), and 0.046 ($K/k = 1.13$, $d = 9\,\mu\text{m}$). Contrastingly, the simulated values of σ_{eff} seem to increase gradually even at the lowest values of c, and the percolation thresholds, if any, are hard to detect. This situation is typical of conductivity simulations for finite-size systems where the percolation threshold is a random non-Gaussian variable [71].

C. Testing our model for the case of uniform penetrable shells

This step consists in fitting conductivity data [44,46] using Eq. (40) with $\phi = \phi(c, \delta)$ given by Eq. (45) and δ given by Eq. (46). As Fig. 5 demonstrates, the value of $K \approx 1.07k$, determined by fitting the composition data [46] (step A), is also appropriate to reproduce conductivity data [46] (this step). Similarly, Figs. 6 and 7 clearly indicate that the parameter K alone, with a reasonable fitting value for each series, is sufficient to reproduce all ten series of simulation data [46] for σ_{eff} of dispersions of particles with uniform penetrable shells. This fact is a strong argument in favor of the model expressed by Eqs. (40) and (45).
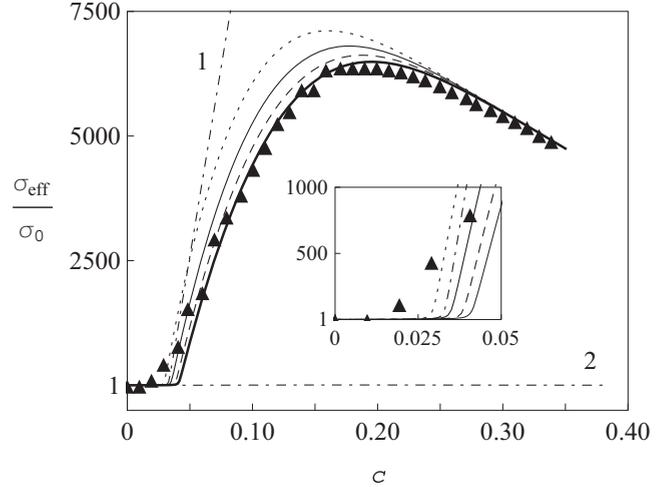

FIG. 5. Simulation data [46] for σ_{eff} as a function of c at $t = 5\,\mu\text{m}$ and $d = 7\,\mu\text{m}$ (▲), and their fits by Eq. (40) with $\phi(c, \delta)$ given by Eq. (45) for the values of δ from Fig. 2 (dotted, dashed, and solid lines) and $K = 1.03\,k$ (thick solid line). The dotdashed lines: the result for σ_{eff} given by Eq. (40) with $\phi(c, \delta)$ for hard shells [see Eq. (31)] and $K = 1.07k$ (line 1); that by the Maxwell-Garnett-type Eq. (44) with $\phi(c, \delta)$ given by Eq. (45) and $K = 1.03k$ (line 2). Note that: both results fail to reproduce data [46]; line 2 has a maximum of $x_{\text{eff}} \approx 7.2$ at $c \approx 0.17$ which cannot be resolved in this figure.

D. Scrutinizing the conductivity maximum positions

Under the condition $\sigma_1 \ll \sigma_0 \ll \sigma_2$, typical of simulations [44,46], Eq. (40) can be greatly simplified by passing to the limit $\sigma_1 \to 0$ where it takes the form

$$4\sigma_{\text{eff}}^3 - 2[(2 - 3\phi)\sigma_0 - (1 + 3c - 3\phi)\sigma_2]\sigma_{\text{eff}}^2$$
$$- (2 - 3c)\sigma_0\sigma_2\sigma_{\text{eff}} = 0. \quad (47)$$
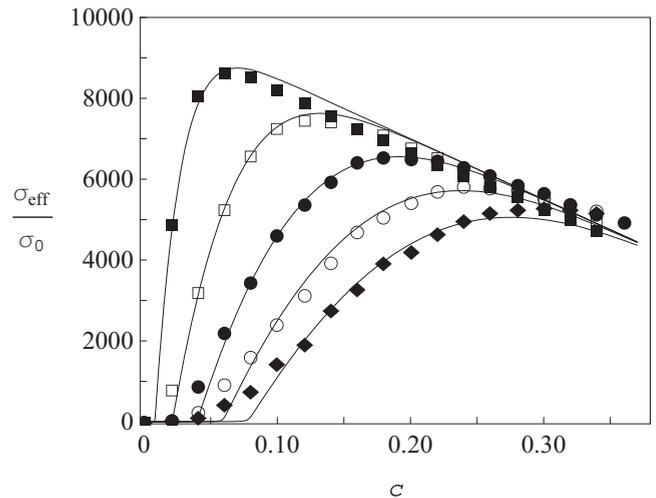

FIG. 6. Simulation results [44] for σ_{eff} as a function of c for a fixed shell thickness $t = 5\,\mu\text{m}$, constant shell conductivity, and grain diameters $d = 3$ (■), 5 (□), 7 (●), 9 (○), and $11\,\mu\text{m}$ (♦). Solid lines: our theory results for δ's given by Eq. (46) with $K = k$, $1.05\,k$, $1.05\,k$, $1.07\,k$, and $1.10\,k$, respectively.
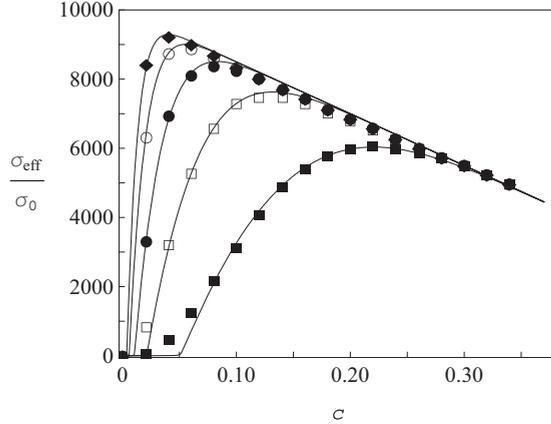
FIG. 7. Simulation results [44] for σ_{eff} as a function of c for a fixed grain diameter $d = 5\,\mu m$, constant shell conductivity, and shell thicknesses $t = 3$ (■), 5 (□), 7 (●), 9 (○), and $11\,\mu m$ (♦). Solid lines: our theory results for δ's given by Eq. (46) with $K = 1.08\,k$, $1.05\,k$, $1.06\,k$, $1.07\,k$, and $1.06\,k$, respectively.

A nontrivial physically meaningful solution to Eq. (47) is

$$\sigma_{eff} = \tfrac{3}{4}(A + \sqrt{B + A^2}),\qquad(48)$$

where

$$A \equiv \left(\tfrac{2}{3} - \phi\right)\sigma_0 + \left(\phi - c - \tfrac{1}{3}\right)\sigma_2,\qquad(49a)$$

$$B \equiv \tfrac{4}{3}\left(\tfrac{2}{3} - c\right)\sigma_0\sigma_2.\qquad(49b)$$

For the data series in Figs. 6 and 7, the σ_{eff} versus c plots given by Eqs. (48) and (40) are indistinguishable.

The concentrations c_{max} where the conductivity maxima occur are found from the conditions $\partial\sigma_{eff}/\partial c = 0$ and $\partial^2\sigma_{eff}/\partial c^2 < 0$. Since near these maxima $\sigma_{eff} \gg \sigma_0$, it follows from Eq. (47) and the first condition that

$$\partial\phi(c,\delta)/\partial c\,|_{c=c_{max}} = 1,\qquad(50)$$

and that the derivatives $\partial^2\sigma_{eff}/\partial c^2$ and $\partial^2\phi/\partial c^2$ have the same sign at $c = c_{max}$. According to Eq. (45), $\partial^2\phi/\partial c^2 < 0$ for $\delta > 0$. So, for such a δ, the second condition is fulfilled, and σ_{eff} has a local maximum at c_{max} indeed. Its value σ_{max} is given by Eqs. (48) at $c = c_{max}$ found from Eq. (50).

The c_{max} versus δ dependence given by Eqs. (50) and (45) is shown in Fig. 8. It agrees very well with every pair of c_{max} and δ obtained by processing simulation data [44] with Eqs. (40), (45), and (46). This fact signifies the internal consistency of our processing procedure. The dependence of σ_{max} on the grain diameter d (and, in fact, δ) is tested in Fig. 9. It is seen that our theory reproduces almost the entire set of simulations data [44]. Noticeable discrepancies occur only for smallest values of δ where the simulation errors are of the greatest magnitude.

It is worthy of note that, provided $\sigma_1 \ll \sigma_0 \ll \sigma_2$, Eq. (50) and the inequality $\partial^2\phi/\partial c^2|_{c=c_{max}} < 0$ can be viewed as the second derivative test for a local maximum of the shell volume concentration $\phi(c,\delta) - c$. If the shells are penetrable, then this maximum was shown to occur at c_{max}. In contrast, there is no such a maximum, and therefore no local maximum for σ_{eff} given by Eq. (40), in the case of hard shells, where
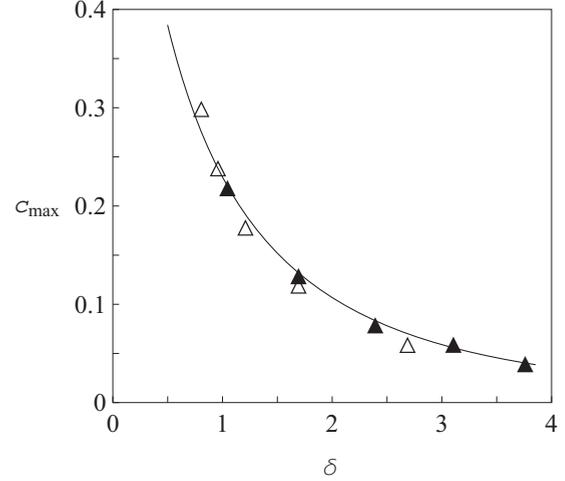

FIG. 8. c_{max} as a function of δ according to Eqs. (50) and (45) (solid line). The empty (△) and filled (▲) triangles: the c_{max} values recovered from simulation results [44] shown in Figs. 6 and 7, respectively; the corresponding δ values were estimated by Eq. (46).

$\phi(c,\delta)$ is expressed by Eq. (31) (see Fig. 5). One way out of this situation is based on the idea [72,73] to replace the conductivities σ_q of the constituents by certain conductivities σ_q^* depending on not only σ_q, but also an averaged property of the surrounding medium in some form. In applications [40–42] to CSEs, this approach is realized in several steps: (1) introducing different quasi-two-phase models of CSEs for the limiting cases of low and high values of c; (2) calculating the effective conductivities in both limiting models by standard one-particle methods; (3) sewing the solutions at some characteristic concentration v_2^*, where the maximum of σ_{eff} is observed. Evidently, v_2^* serves as a fitting parameter, and the dependence of σ_{eff} upon c reveals a nonphysical cusp at $c = v_2^*$ (see Refs. [40–42]).
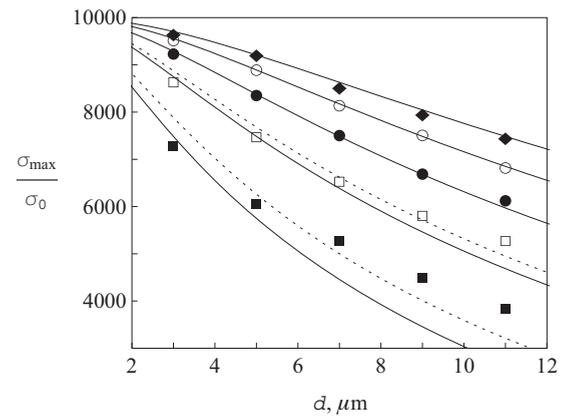

FIG. 9. Simulation results [44] for σ_{max} as a function of the grain diameter d for a constant shell conductivity and shell thicknesses $t = 3$ (■), 5 (□), 7 (●), 9 (○), and $11\,\mu m$ (♦). Solid lines: our theory results for σ_{max} given by Eqs. (48), (50), and (46) with $K = k$. Dotted lines: the same for $t = 3$ and $5\,\mu m$ at $K = 1.15\,k$ and $1.07\,k$, respectively.

E. Testing our model for the case of inhomogeneous penetrable shells

Now, simulation results [45] for σ_{eff} are processed with Eq. (43). The shell conductivity σ_2' was assumed in Ref. [45] to be distributed by a spherically symmetric Gaussian law, with a maximum of σ_{max}' at the distance $t/2$ from the surface of the grain and a minimum of σ_{min}' on the outer border of the shell (see Table I for the numerical values). The explicit expression for $\sigma_2' = \sigma_2'(u)$ was not reported, and neither was the rule whereby a particular conductivity value was assigned to each cubic cell belonging to the shell.

Based on the above description, suppose that

$$\sigma_2'(u) = \sigma_{\text{max}}' \exp\left[-\frac{4(u - \delta'/2)^2}{\delta'^2} \ln\left(\frac{\sigma_{\text{max}}'}{\sigma_{\text{min}}'}\right) \right]. \quad (51)$$

Let $n = t/a$ be the (even) number of the radially-distributed cubic cells inside the shell, with their centers located at points $u_p = (2p - 1)\delta'/2n$, $p = 1, \ldots, n$. If the conductivity of the pth cell is defined as the value of $\sigma_2'(u)$ at u_p, then we can expect that the counterpart of the distribution (51) in our model has the same functional form

$$\sigma_2(u) = \sigma_{\text{max}} \exp\left[-\frac{4(u - \delta/2)^2}{\delta^2} \ln\left(\frac{\sigma_{\text{max}}}{\sigma_{\text{min}}}\right) \right], \quad (52)$$

with σ_{max} and σ_{min} equal to the conductivities of the two central cells and the two outermost cells, respectively:

$$\sigma_{\text{max}} = \sigma_2'(u_{n/2}) = \sigma_2'(u_{n/2+1}) = \sigma_{\text{max}}'\left(\frac{\sigma_{\text{max}}'}{\sigma_{\text{min}}'}\right)^{-1/n^2},$$

$$\sigma_{\text{min}} = \sigma_2'(u_1) = \sigma_2'(u_n) = \sigma_{\text{max}}'\left(\frac{\sigma_{\text{max}}'}{\sigma_{\text{min}}'}\right)^{-(n-1)^2/n^2}.$$
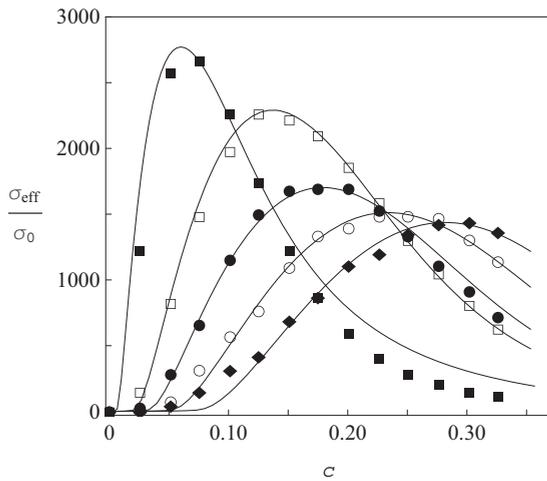
FIG. 10. Simulation results [45] for σ_{eff} as a function of c for a fixed shell thickness $t = 5\,\mu$m, grain diameters $d = 3$ (■), 5 (□), 7 (●), 9 (○), and 11 μm (♦), and Gaussian shell conductivity profiles (51). Solid lines: our theory results for the corresponding δ's and shell conductivity profiles (52), found with the mapping parameters listed in Table II.
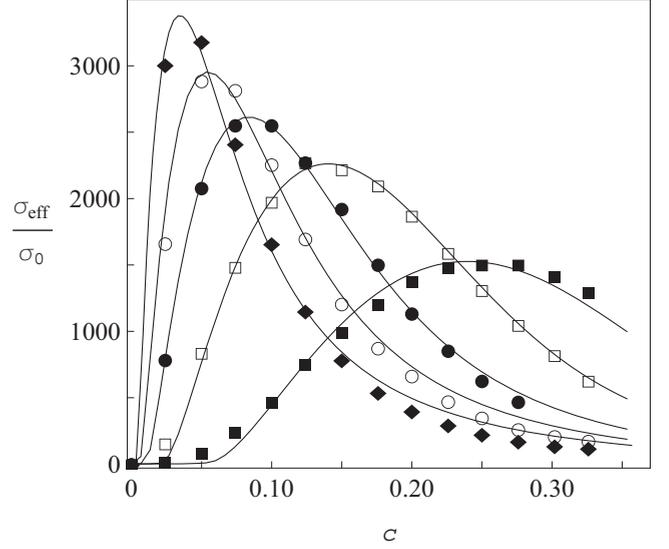
FIG. 11. Simulation results [45] for σ_{eff} as a function of c for a fixed grain diameter $d = 5\,\mu$m, shell thicknesses $t = 3$ (■), 5 (□), 7 (●), 9 (○), and 11 μm (♦), and Gaussian shell conductivity profiles (51). Solid lines: our theory results for the corresponding δ's and shell conductivity profiles (52), found with the mapping parameters listed in Table III.

In the limit $n \to \infty$, $\sigma_{\text{max}} = \sigma_{\text{max}}'$ and $\sigma_{\text{min}} = \sigma_{\text{min}}'$; for any finite n, $\sigma_{\text{max}} < \sigma_{\text{max}}'$, $\sigma_{\text{min}} > \sigma_{\text{min}}'$, and

$$\frac{\sigma_{\text{max}}}{\sigma_{\text{min}}} = \left(\frac{\sigma_{\text{max}}'}{\sigma_{\text{min}}'}\right)^{(n-2)/n}.$$

These results indicate that the conductivity parameters in the distribution (52) are dependent of the details of simulations [45]. In the situation where these details are unknown, one of these parameters, say, σ_{max}, can be treated as a fitting one.

Figures 10 and 11 demonstrate the results of processing data [45] by Eq. (43) with $\phi(c, \delta)$, δ, and $\sigma_2(u)$ given by Eqs. (45), (46), and (52), respectively. The used values of K and σ_{max} are summarized in Tables II and III; for the sake of simplification, it was taken $\sigma_{\text{min}} = \sigma_{\text{min}}'$. As seen, our model is capable of reproducing the simulation data surprisingly well. Note also that according to the above reasoning and for the given $\sigma_{\text{max}}'/\sigma_{\text{min}}' = 100$, $\log_{10}(\sigma_{\text{max}}/\sigma_{\text{min}}) = 2(n - 2)/n$. In the cases $t = 9\,\mu$m ($n = 18$) and $t = 11\,\mu$m ($n = 22$), which are most appropriate for comparisons, this relation gives $\log_{10}(\sigma_{\text{max}}/\sigma_{\text{min}}) \approx 1.78$ and 1.82, respectively. The so-estimated values of $\sigma_{\text{max}}/\sigma_{\text{min}}$ differ from those obtained by fitting by no more than 17 and 12%.

TABLE II. Parameters used to fit the simulation data in Fig. 10 by Eq. (43) with Gaussian shell conductivity profiles (52) at $\sigma_{\text{min}} = \sigma_{\text{min}}'$; $\sigma_0 = 10^{-8}$ S/cm, $\sigma_1 = 10^{-12}$ S/cm.

d, μm	3	5	7	9	11
K/k	1.09	1.02	1.13	1.11	1.09
$\log_{10}(\sigma_{\text{max}}/\sigma_{\text{min}})$	1.83	1.89	1.82	1.88	1.98

TABLE III. Parameters used to fit the simulation data in Fig. 11 by Eq. (43) with Gaussian shell conductivity profiles (52) at $\sigma_{min} = \sigma'_{min}$; $\sigma_0 = 10^{-8}$ S/cm, $\sigma_1 = 10^{-12}$ S/cm.

t, μm	3	5	7	9	11
K/k	1.00	1.00	1.05	1.07	1.13
$\log_{10}(\sigma_{max}/\sigma_{min})$	1.90	1.89	1.85	1.85	1.87

IX. APPLICATION TO EXPERIMENT AND DISCUSSION

To exemplify the efficiency of the theory, we have applied it to Liang's pioneering experimental data [1] for σ_{eff} as a function of c for real LiI/Al$_2$O$_3$ CSEs. The procedure involved several steps. First, we processed data [1] with Eq. (43) assuming the hard cores to be nonconductive (for alumina, $\sigma_1 \approx 1 \times 10^{-14}$ S/cm) and using the following three approximations for the shell conductivity profile $\sigma_2 = \sigma_2(r)$:

(a) uniform shells ($0 < u < \delta_1$),

$$x_2 = \text{const};$$

(b) two-layer shells ($0 < u < \delta_2$),

$$x_2(u) = \begin{cases} x_{2,1} & \text{if} \quad 0 < u < \delta_1, \\ x_{2,2} & \text{if} \quad \delta_1 < u < \delta_2; \end{cases} \quad (53)$$

(c) continuous shells of the sigmoid-type ($u > 0$),

$$x_2(u) = X_{2,1} + \frac{X_{2,2} - X_{2,1}}{1 + \exp\left(-\frac{u - \Delta_1}{\alpha}\right)} + \frac{1 - X_{2,2}}{1 + \exp\left(-\frac{u - \Delta_2}{\alpha}\right)}. \quad (54)$$

Here: $x_2 = \sigma_2/\sigma_0$ and $x_{2,i} = \sigma_{2,i}/\sigma_0$ are the relative conductivities, and δ_1 and δ_2 are the relative thicknesses of the layers;
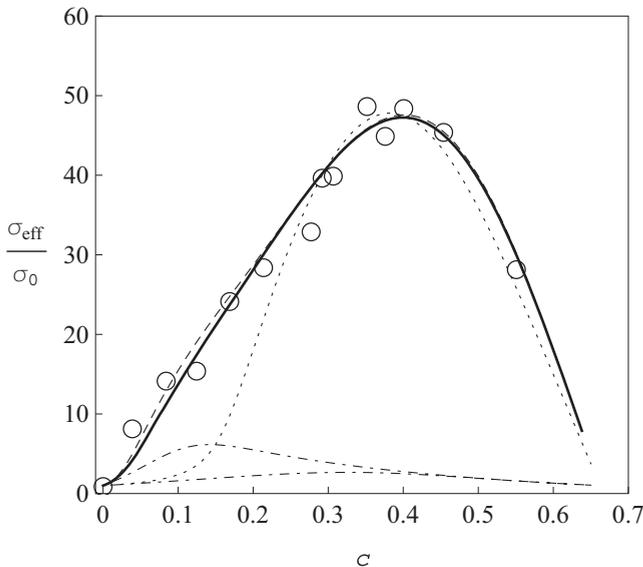

FIG. 12. Experimental data [1] (○) for σ_{eff} of LiI/Al$_2$O$_3$ CSEs and their fits using (a) uniform shell (40) (dotted line), (b) two-layer (53) (dashed line), and (c) sigmoid-type (54) (solid line) approximations for $\sigma_2(r)$. The fitting parameters are listed in Table IV. The corresponding shell conductivity profiles are shown in Fig. 13. The dotdashed lines illustrate the predictions by the Maxwell-Garnett-type mixing rules (44) for the same approximations (a) (lower line) and (b) (upper line) and the same parameters, indicated in Table IV.
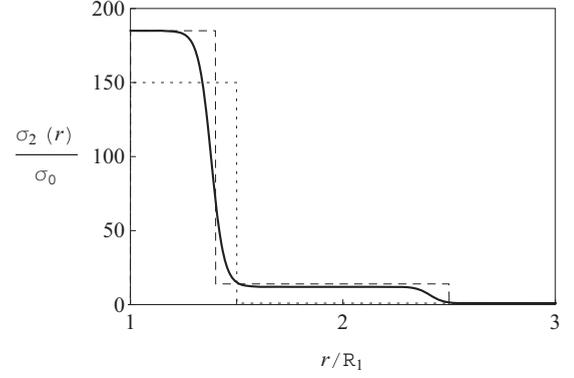

FIG. 13. The shell conductivity profiles corresponding to the fits shown in Fig. 12.

$X_{2,1}$, $X_{2,2}$, Δ_1, and Δ_2 are the parameters of the generating function (54). In the limit $\alpha \to 0$, where the latter takes form (53), they become equal to the parameters $x_{2,1}$, $x_{2,2}$, δ_1, and δ_2 of the two-layer model, respectively.

When processing the data with profile (54), its parameters were varied so as to smoothen it as much as possible; the parameter δ_M in Eq. (43) was fixed at a value of 5, for a further increase of it did not affect the results.

The processing results are presented in Figs. 12, 13, and Table IV. A good agreement between the theory and experiment is achievable under the condition that $\sigma_2(r)$ consists of two distinct parts. To gain insight into this fact, we note that the use of penetrable shells is a convenient way of modeling the effective microstructure and conductivity of a system. Their $\sigma_2(r)$ is not equivalent to the actual conductivity distributions around the hard cores, but is used to analyze these distributions and possible mechanisms behind them.

Consider, for instance, model (53), which adequately describes the entire set of data [1]. For this model, Eq. (43) can be represented as the system of two equations

$$[1 - \phi(c, \delta_1)] \frac{\sigma_0^* - \sigma_{eff}}{2\sigma_{eff} + \sigma_0^*} + c \frac{\sigma_1 - \sigma_{eff}}{2\sigma_{eff} + \sigma_1}$$

$$+ [\phi(c, \delta_1) - c] \frac{\sigma_{2,1} - \sigma_{eff}}{2\sigma_{eff} + \sigma_{2,1}} = 0, \quad (55)$$

$$[1 - \phi(c, \delta_1)] \frac{\sigma_0^* - \sigma_{eff}}{2\sigma_{eff} + \sigma_0^*} = [1 - \phi(c, \delta_2)] \frac{\sigma_0 - \sigma_{eff}}{2\sigma_{eff} + \sigma_0}$$

$$+ [\phi(c, \delta_2) - \phi(c, \delta_1)] \frac{\sigma_{2,2} - \sigma_{eff}}{2\sigma_{eff} + \sigma_{2,2}}. \quad (56)$$

TABLE IV. Parameters used to fit experimental data [1] for σ_{eff} of LiI/Al$_2$O$_3$ CSEs using (a) uniform shell (40), (b) two-layer (53), and (c) sigmoid-type (54) approximations for $\sigma_2(r)$; $\sigma_0 = 2.5 \times 10^{-7}$ S/cm, $x_1 = 0$.

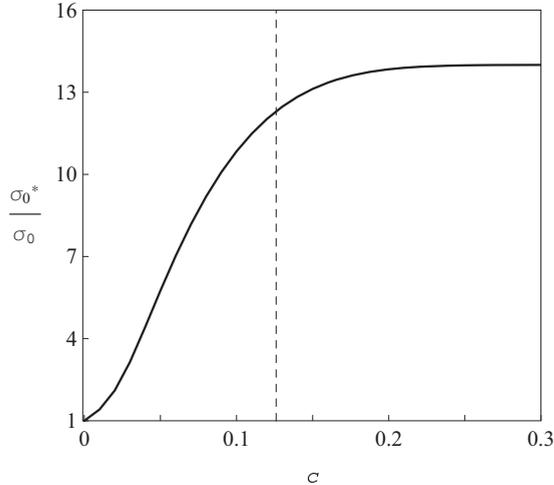| (a)	x_2	δ			
	150	0.5			
(b)	$x_{2,1}$	$x_{2,2}$	δ_1	δ_2	
	185	14	0.40	1.50	
(c)	$X_{2,1}$	$X_{2,2}$	Δ_1	Δ_2	α
	185	12	0.38	1.41	0.03

FIG. 14. The matrix conductivity σ_0^* as a function of c (solid line), as recovered from Eq. (56) for the two-shell profile shown in Fig. 13 (and its parameters given in row (b) in Table IV). Dashed line: the percolation threshold $c_c \approx 0.126$ in the system of the inner shells.

Under the conditions c, $\phi(c, \delta_1) \ll \phi(c, \delta_2) < 1$, the estimate $\sigma_{\text{eff}} \approx \sigma_0^*$ holds true [see Eq. (55)], σ_{eff} is basically a function of σ_0, c, δ_2, and $\sigma_{2,2}$ [see Eq. (56)], and so is σ_0^*. In other words, at low c and $\phi(c, \delta_1)$, the electrical conduction in the system is determined by σ_0^*, which is formed mainly by the outermost part of $\sigma_2(r)$.

Physically, in view of Eq. (55), σ_0^* can be interpreted as the effective conductivity of the host matrix in the CSE prepared by embedding filler particles with hard cores, of radius R_1 and conductivity σ_1, and penetrable shells, of relative thickness δ_1 and conductivity $\sigma_{2,1}$, into this matrix. The dependence of σ_0^* on c can be recovered from Eq. (56) and, for LiI/Al$_2$O$_3$ CSEs [1], is shown in Fig. 14. For $c \lesssim 0.1$, it very closely resembles the initial part of the σ_{eff} versus c plot in Fig. 12. This signifies that, despite being highly-conductive, the above shells [inner layers in $\sigma_2(r)$] practically do not contribute to σ_{eff} of LiI/Al$_2$O$_3$ CSEs in this concentration range.

Note that matrix processes enhancing the conductivity of the matrix conductors in CSEs may include: a formation of defect-rich space charge regions near the grain boundaries in a polycrystalline matrix [74]; development of a highly conductive network of piled-up dislocations caused by mechanically- and thermally-induced misfits [75–77]; fast ionic transport along matrix grain boundaries and/or dislocations [78,79]; homogeneous doping of the matrix through the dissolution of impurities and very fine particles in it [80–82].

The situation changes drastically in the vicinity of the percolation threshold c_c for the indicated core-shell particles. The value of c_c is found from the relation $\phi(c_c, \delta_1) = 1/3$ [66], which for $\delta_1 = 0.4$ gives $c_c \approx 0.126$. It is the inner part in $\sigma_2(r)$ that forms σ_{eff} at $c \gtrsim c_c$.

Typical examples of interfacial processes giving rise to highly conductive regions around the filler particles are: a formation, through preferential ion adsorption (desorption) at the particle-matrix interface, of a space-charge layer enriched with point defects [83–85]; rapid ion transport along the

particle-matrix interface due to matrix lattice distortions near it [78,86]; stabilization of conductive nonequilibrium states by the adjacent filler particles [87,88]; formation of a new "superstructure" or interphase due to chemical reactions at the interface [89]. For LiI/Al$_2$O$_3$ CSEs, the inner part in $\sigma_2(r)$ can be associated with a space charge layer. Indeed, our values $\delta_1 = 0.4$ and $x_{2,1} = 185$ correlate well with Jiang and Wagner's estimates $\delta = 0.4$ and $x_2 = 324$ [30,31] for the relative thickness and relative conductivity of the space charge layer in LiI/Al$_2$O$_3$ CSEs modeled as cubic lattices with ideal random distributions of cubic filler particles; estimates [30,31] were obtained by a method of combination of a percolation model with the space charge layer model.

For other types of composites, alternative physicochemical mechanisms are expected to come into play. In particular, Eq. (43) is sufficient [67] to describe the observed behavior of σ_{eff} for composite polymeric electrolytes (CPEs) based on poly(ethy1ene oxide) (PEO) and oxymethylene-linked PEO (OMPEO), provided the pertinent $\sigma_2(r)$ consists of several parts. These account for: a change of the matrix's conductivity in the course of preparation of the composites [the outermost part in $\sigma_2(r)$]; amorphization of the polymer matrix by filler grains (the central part); a stiffening effect of the filler on the amorphous phase and effects caused by irregularities in the shape of the filler grains (the innermost part).

It can be concluded from the above results that the functional form (43) for σ_{eff} in terms of the parameters of the hard-core-penetrable-shell model is highly flexible and rather universal in the sense of being applicable to various dispersed systems. At the same time, the values of these parameters are not universal because of a diversity of physico-chemical mechanisms that not only form σ_{eff} of real composite materials, but also alter the properties of their constituents themselves. Consequently, these values can be estimated provided that sufficiently extensive experimental data are available.

The predictive power of the theory can be significantly increased and, therefore, the amount of the required experimental work considerable decreased by going beyond the limits of a pure homogenization theory and employing certain model estimates for the constituent's parameters and their dependences on various factors, say, temperature. For instance, to recover the temperature behavior of σ_{eff} for OMPEO-based CPEs with different concentrations of polyacrylamide filler, it is sufficient to use a three-layer structure for $\sigma_2(r)$, assume the conductivities of the layers and the matrix to obey, as functions of temperature, the empirical three-parametric Vogel-Tamman-Fulcher (VTF) equation, and recover the VTF parameters for these conductivities by processing only three conductivity isotherms for the CPEs. The reader is referred to Ref. [67] for the details.

X. CONCLUSION

The main results of this paper are as follows:

(i) We give a self-consistent analytic solution to the problem of the effective quasistatic electrical conductivity σ_{eff} of a statistically homogeneous and isotropic dispersion of hard-core–penetrable-shell particles with radially symmetrical, piecewise-continuous shell conductivity profile $\sigma_2(r)$; the local conductivity value in the dispersion is assumed to be

determined by the distance from the point of interest to the nearest particle. The solution effectively incorporates many-particle effects in concentrated dispersions and is obtained by: (a) generalizing the compact group approach [48–51] to systems with complex-valued permittivities of the constituents; (b) deriving the governing equation (24) for the effective quasistatic complex permittivity $\hat{\varepsilon}_{eff}$ of the system; and (c) requiring that the boundary condition [55] for the normal components of complex electric fields in conducting dielectrics be satisfied. With the latter requirement fulfilled, Eq. (24) becomes a closed relation for $\hat{\varepsilon}_{eff}$ in terms of the statistical moments for the local deviations of the complex permittivity distribution in the model dispersion from $\hat{\varepsilon}_{eff}$.

(ii) The desired σ_{eff}, extracted from Eq. (26), is a functional of the constituents' conductivities and volume concentrations that obeys the integral relation (43). For the model under consideration, this relation is expected to be rigorous in the limit of static probing fields. The volume concentrations account for the statistical microstructure of the system. They are determined by statistical averages of products of the particles' characteristic functions and can be estimated using other authors' analytical [20,52] and numerical [53,54] results for the volume concentration of uniform shells.

(iii) The validity of the solution, at least for the parameter values typical of CSEs and CPEs, is demonstrated by the results of (a) mapping it onto extensive RRN simulation data [44–46] for the composition and σ_{eff} of 3D dispersions comprising a poorly-conductive, uniform matrix and isotropic particles with nonconductive, hard cores and highly-conductive, fully-penetrable shells with different $\sigma_2(r)$; and (b) applying it to pioneering experimental data [1] for real LiI/Al$_2$O$_3$ CSEs. The latter results also clarify the meaning of $\sigma_2(r)$, reveal the role of its different parts in the formation of σ_{eff}, and indicate that both matrix and interfacial processes contribute to enhanced electrical conduction in LiI/Al$_2$O$_3$ CSEs.

To conclude, we note that Eqs. (24) and (43) have already been shown to efficiently describe electric percolation phenomena in random composites [66], electrical conductivity of suspensions of insulating nanoparticles [90], and that of CPEs [67].

ACKNOWLEDGMENTS

[1] C. C. Liang, J. Electrochem. Soc. **120**, 1289 (1973).

[2] J. B. Wagner, Jr., Mater. Res. Bull. **15**, 1691 (1980).

[3] J. B. Wagner, Jr., Composite solid ion conductors, in *High Conductivity Solid Ionic Conductors, Recent Trends and Applications*, edited by T. Takahashi (World Scientific, Singapore, 1989), pp. 146–165.

[4] N. J. Dudney, Annu. Rev. Mater. Sci. **19**, 103 (1989).

[5] J. Maier, Prog. Solid State Chem. **23**, 171 (1995).

[6] R. C. Agrawal and R. K. Gupta, J. Mater. Sci. **34**, 1131 (1999).

[7] N. F. Uvarov, J. Solid State Electrochem. **15**, 367 (2011).

[8] N. F. Uvarov, Composite solid electrolytes, in *Solid State Electrochemistry II: Electrodes, Interfaces and Ceramic Membranes*, edited by V. V. Kharton (Wiley-VCH Verlag GmbH & Co. KGaA, Weinheim, Germany, 2011), Chap. 2, pp. 31–71.

[9] J. Gao, Y.-S. Zhao, S.-Q. Shi, and H. Li, Chin. Phys. B **25**, 018211 (2016).

[10] W. Wieczorek and M. Siekierski, Composite Polymeric Electrolytes, in *Nanocomposites, Ionic Conducting Materials and Structural Spectroscopies*, edited by P. Knauth and J. Schoonman (Springer, New York, 2008), pp. 1–70.

[11] *Polymer Electrolytes, Fundamentals and Applications*, edited by C. Sequeira and D. Santos (Woodhead Publishing, Cambridge, 2010).

[12] J. C. Maxwell, *A Treatise on Electricity and Magnetism*, 1st ed., Vol. 1 (Clarendon Press, Oxford, 1873), pp. 362–365.

[13] J. C. M. Garnett, Philos. Trans. R. Soc. London A **203**, 385 (1904).

[14] D. Bruggeman, Ann. Phys. (Leipzig) **24**, 636 (1935).

[15] R. Landauer, J. Appl. Phys. **23**, 779 (1952).

[16] C. F. Bohren and D. R. Huffman, *Absorption and Scattering of Light by Small Particles* (J. Wiley & Sons, New York, 1983).

[17] D. J. Bergman and D. Stroud, Solid State Phys. **46**, 147 (1992).

[18] A. Sihvola, *Electromagnetic Mixing Formulas and Applications* (The Institution of Engineering and Technology, London, 1999).

[19] L. Tsang and J. A. Kong, *Scattering of Electromagnetic Waves: Advanced Topics* (J. Wiley & Sons, New York, 2001).

[20] S. Torquato, *Random Heterogeneous Materials: Microstructure and Macroscopic Properties* (Springer Science+Business Media, New York, 2002).

[21] G. W. Milton, *The Theory of Composites* (Cambridge University Press, Cambridge, 2004).

[22] S. Torquato, J. Chem. Phys. **81**, 5079 (1984).

[23] S. Torquato, J. Chem. Phys. **83**, 4776 (1985).

[24] S. Torquato, J. Appl. Phys. **58**, 3790 (1985).

[25] V. Myroshnychenko and C. Brosseau, Phys. Rev. E **71**, 016701 (2005).

[26] V. Myroshnychenko and C. Brosseau, J. Appl. Phys. **97**, 044101 (2005).

[27] V. Myroshnychenko and C. Brosseau, J. Phys. D: Appl. Phys. **41**, 095401 (2008).

[28] V. Myroshnychenko and C. Brosseau, Phys. B: Condens. Matter **405**, 3046 (2010).

[29] J. C. Wang and N. J. Dudney, Solid State Ionics **18-19**, 112 (1986).

[30] S. Jiang and J. B. Wagner, Jr., J. Phys. Chem. Solids **56**, 1101 (1995).

[31] S. Jiang and J. B. Wagner, Jr., J. Phys. Chem. Solids **56**, 1113 (1995).

[32] A. Bunde, W. Dieterich, and E. Roman, Phys. Rev. Lett. **55**, 5 (1985).

[33] H. E. Roman, A. Bunde, and W. Dieterich, Phys. Rev. B **34**, 3439 (1986).

[34] R. Blender and W. Dieterich, J. Phys. C: Solid State Phys. **20**, 6113 (1987).

[35] A. G. Rojo and H. E. Roman, Phys. Rev. B **37**, 3696 (1988).

[36] H. E. Roman and M. Yussouff, Phys. Rev. B **36**, 7285 (1987).

[37] H. E. Roman, J. Phys.: Condens. Matter **2**, 3909 (1990).

[38] A. M. Stoneham, E. Wade, and J. A. Kilner, Mater. Res. Bull. **14**, 661 (1979).

[39] A. D. Brailsford, Solid State Ionics **21**, 159 (1986).

[40] C.-W. Nan and D. M. Smith, J. Mater. Sci. Lett. **10**, 1142 (1991).

[41] C.-W. Nan and D. M. Smith, Mater. Sci. Eng. B **10**, 99 (1991).

[42] C.-W. Nan, Prog. Mater. Sci. **37**, 1 (1993).

[43] W. Wieczorek, K. Such, Z. Florjanczyk, and J. R. Stevens, J. Phys. Chem. **98**, 6840 (1994).

[44] M. Siekierski and K. Nadara, Electrochim. Acta **50**, 3796 (2005).

[45] M. Siekierski, K. Nadara, and P. Rzeszotarski, J. New Mat. Electrochem. Systems **9**, 375 (2006).

[46] M. Siekierski and K. Nadara, J. Power Sources **173**, 748 (2007).

[47] S. Kalnaus, A. S. Sabau, S. Newman, W. E. Tenhaeff, C. Daniel, and N. J. Dudney, Solid State Ionics **199–200**, 44 (2011).

[48] M. Ya. Sushko, Zh. Eksp. Teor. Fiz. **132**, 478 (2007) [JETP **105**, 426 (2007)].

[49] M. Ya. Sushko and S. K. Kris'kiv, Zh. Tekh. Fiz. **79**, 97 (2009) [Tech. Phys. **54**, 423 (2009)].

[50] M. Ya. Sushko, J. Phys. D: Appl. Phys. **42**, 155410 (2009).

[51] M. Ya. Sushko, Phys. Rev. E **96**, 062121 (2017).

[52] P. A. Rikvold and G. Stell, J. Chem. Phys. **82**, 1014 (1985); J. Colloid Interface Sci. **108**, 158 (1985).

[53] S. B. Lee and S. Torquato, J. Chem. Phys. **89**, 3258 (1988).

[54] M. Rottereau, J. C. Gimel, T. Nicolai, and D. Durand, Eur. Phys. J. E **11**, 61 (2003)

[55] R. W. Sillars, J. Inst. Electr. Eng. **80**, 378 (1937).

[56] Yu. A. Ryzhov, V. V. Tamoikin, and V. I. Tatarskii, Zh. Exp. Teor. Phys. **48**, 656 (1965) [Sov. Phys. JETP **21**, 433 (1965)].

[57] W. Weiglhofer, Am. J. Phys. **57**, 455 (1989).

[58] Yu. A. Ryzhov and V. V. Tamoikin, Izv. VUZ., Radiofiz. **13**, 356 (1970) [Radiophys. Quantum Electron. **13**, 273 (1970)].

[59] V. V. Tamoikin, Izv. VUZ., Radiofiz. **14**, 285 (1971) [Radiophys. Quantum Electron. **14**, 228 (1971)].

[60] L. Tsang and J. A. Kong, Radio Sci. **16**, 303 (1981).

[61] N. P. Zhuck, Phys. Rev. B **50**, 15636 (1994).

[62] B. Michel and A. Lakhtakia, Phys. Rev. E **51**, 5701 (1995).

[63] T. G. Mackay, A. Lakhtakia, and W. S. Weiglhofer, Phys. Rev. E **62**, 6052 (2000); **63**, 049901(E) (2001).

[64] T. G. Mackay, A. Lakhtakia, and W. S. Weiglhofer, Phys. Rev. E **64**, 066616 (2001).

[65] B. M. Ross and A. Lakhtakia, Microw. Opt. Technol. Lett. **44**, 524 (2005).

[66] M. Ya. Sushko and A. K. Semenov, Condens. Matter Phys. **16**, 13401 (2013).

[67] M. Ya. Sushko and A. K. Semenov, J. Mol. Liq. **279**, 677 (2019).

[68] H. Reiss, H. L. Frisch, and J. L. Lebowitz, J. Chem. Phys. **31**, 369 (1959).

[69] S. Kirkpatrick, Phys. Rev. Lett. **27**, 1722 (1971).

[70] S. Kirkpatrick, Rev. Mod. Phys. **45**, 574 (1973).

[71] L. Berlyand and J. Wehr, Commun. Math. Phys. **185**, 73 (1997).

[72] M. Nakamura, J. Phys. C: Solid State Phys. **15**, L749 (1982).

[73] M. Nakamura, Phys. Rev. B **29**, 3691 (1984).

[74] J. Maier, Ber. Bunsenges. Phys. Chem. **90**, 26 (1986).

[75] N. J. Dudney, J. Am. Ceram. Soc. **70**, 65 (1987).

[76] N. J. Dudney, Solid State Ionics **28–30**, 1065 (1988).

[77] S. Mühlherr, K. Läuger, E. Schreck, K. Dransfeld, and N. Nicoloso, Solid State Ionics **28–30**, 1495 (1988).

[78] J. B. Phipps, D. L. Johnson, and D. H. Whitmore, Solid State Ionics **5**, 393 (1981).

[79] A. Atkinson, Solid State Ionics **28-30**, 1377 (1988).

[80] T. L. Wen, R. A. Huggins, A. Rabenau, and W. Weppner, Rev. Chim. Miner. **20**, 643 (1983).

[81] R. Dupree, J. R. Howells, A. Hooper, and F. W. Poulsen, Solid State Ionics **9–10**, 131 (1983).

[82] N. J. Dudney, J. Am. Ceram. Soc. **68**, 538 (1985).

[83] T. Jow and J. B. Wagner Jr., J. Electrochem. Soc. **126**, 1963 (1979).

[84] J. Maier, Phys. Status Solidi B **123**, K89 (1984); **124**, K187 (1984).

[85] J. Maier, J. Phys. Chem. Solids **46**, 309 (1985).

[86] J. B. Phipps and D. H. Whitmore, Solid State Ionics **9–10**, 123 (1983).

[87] J. Płocharski and W. Wieczorek, Solid State Ionics **28–30**, 979 (1988).

[88] W. Wieczorek, K. Such, H. Wyciślik, and J. Płocharski, Solid State Ionics **36**, 255 (1989).

[89] J. A. Schmidt, J. C. Bazán, and L. Vico, Solid State Ionics **27**, 1 (1988).

[90] M. Ya. Sushko, V. Ya. Gotsulskiy, and M. V. Stiranets, J. Mol. Liq. **222**, 1051 (2016).